Journal of Chemical Health Risks

www.jchr.org

JCHR (2025) 15(5), 2559-2570 | ISSN:2251-6727

In Vitro Antimicrobial Antibiofilm Efficacy of Econanosilver Against Uropathogenic Bacteria

Shivani Kumari[1], Ruchika Bhadani[2], Abhishek Kumar[2], Divya Shrivastava[2], Swati Verma[2], Uzma Patel[2], Kratika Pathak[2]

[1]Shridhar University, Pilani, Rajasthan

[2]School of Life and Basic Sciences, Jaipur National University, Jaipur, India

(Received: 25 August 2025 Revised: 27 September 2025 Accepted: 14 October 2025)

KEYWORDS

Urinary tract infection, nanoparticles, *Costus igneus,* Phyto-fabricated, Nano-particles

ABSTRACT:

In recent times, nanoparticles are widely used for combating antibiotic resistance in urinary tract infections (UTIs). Here we have discussed various metal oxide and other nanoparticles and their different formation techniques including organic, nanodiamonds, chemical and green-synthesized inorganic, and composite materials. We have also compared there in vivo and in vitro effects against UTI in both male and females. The study also discusses the antibiofilm property of *Costus igneus* plant extract made in AgNPs against UTI enterococcal isolates. Biofilm formation property of bacteria makes them drug resistant and making UTI difficult to treat. *Costus igneus* AgNPs, having an average size of 65-150nm, showed potent antibacterial activity which also reduces biofilm formation by 81% as compared to other controls. 37.64, 725.7, and 61.08 µg/ml were the results of antimicrobial activity of MIC. Green synthesis of NPs is contributing to a safe and green environment reducing the toxic release

1. Introduction

Urinary Tract Infection or cystitis (bladder infection) and phylonephritis (kidney infection) are caused by bacteria, certain fungi and virus. UTIs are caused by *Escherichia coli*, Gram positive cocci which includes *Staphylococcus* species gaining biofilm properties. UTI can be symptomatic or asymptomatic and about 40% women and 12% of men suffers from UTI once in their lifetime [1]. Uncomplicated UTI is one of the common diseases having 4.49 billion cases in 2024, and at the end of this year, it is subjected to increase by 63.4% (2025) capturing a 54.7% of the market [2]. The global market of Urinary Tract Infection (UTI) is projected to reach USD 12,865 million by the end of 2025 and it is subjected that UTI market can increase by 5.6 CAGR by the year 2034[3]. Cost can increase with high-level antibiotic resistance and *Clostridium* difficile colitis. The resistant of bacteria is mainly caused by biofilm formation[4]. These cells are resistant to both conventional antibiotic treatment and the host's immune system, this causes the reappearance of the infection. Biofilm infections are mainly caused due to intrauterine catheters, pacemakers, and stents and in cystic fibrosis (CF), these all are the foreign bodies that gets infected with biofilm- growing mucoid strains of *Pseudomonas aeruginosa.* Bacteria contains carbapenems, chloramphenicol acetyltransferases enzymes responsible for degradation of multiple antibiotics, such as macrolides, β-lactams, aminoglycosides and phenicol[5]. The combination of drugs also makes bacteria resistant due to their MDR (multi drug resistant) property. Multi-drug efflux pumps are responsible for multidrug resistant. These pumps work together with resistance (R) plasmids or transposons providing resistance to a specific agent[6].

Journal of Chemical Health Risks
www.jchr.org
JCHR (2025) 15(5), 2559-2570 | ISSN:2251-6727

Commonly prescribed antibiotics to treat UTI include trimethoprim-sulfamethoxazole, nitrofurantoin, and ciprofloxacin. The complicated UTIs can lead to severe kidney infection thus proper identification of pathogen is important. However, combining different antibiotics for the treatment often leads to longer diagnosis and increase the chance of reoccurrence[7]. In recent advancement, as nanotechnology is gaining worldwide recognition, and for UTI treatment, nanoparticles (NPs) are contemplating treatment. NPs are capable of targeting bacterial biofilms the problem arises with resistance mechanisms, and is ineffective against bacteria. However, silver nanoparticles (AgNPs) contain antibacterial properties and can provide promising treatment against pathogenic bacteria. There are numerous of plants proven to be effective against bacteria. To form an effective biofilm inhibitor, *Costus igneus* plant or insulin plant extract is being studied with NP along with the antimicrobial properties of silver.

2. Methods

2.1 Sample collection

The fresh and growing leaves of *Costusi gneus* were assembled from botanical garden of Jaipur National University, Jaipur, India in the month of January 2024.The leaves along with the stem were stored in a plastic bag and bought to central laboratory in the basement for further processing[8].

2.2. Isolation of Uropathogenic- The study was conducted at Jaipur National University, Jaipur. The samples were collected from washroom and sewage. Total samples 20 were collected from washroom Jaipur National University Hospital. Each swab of sample was streaked on different media i.e. nutrient, blood, and MacConkey agar, EMB agar. All plates were then incubated at 37 degrees Celsius for 48 hours. The samples were then observed for bacterial colonial characteristics. Identification was then done by their morphological and biochemical characteristics. Further Gram staining was performed for further recognition[9].

2.3 Biofilm Formation- To assess biofilm formation through the colorimetric assay, 96-well titer plate were used. 2 l of each suspended strain were added and incubated for overnight. After the incubation different steps were followed including:

STEP 1: initial condition, in which the medium was removed.

STEP 2: pre-washing, microtiter plate was washed three times with 200 microliters of PBS buffer (0.1 M, pH 7.4) and permit to dry for 15 min. STEP 3: post-washing, staining of wells were done using 200ll of 0.4% crystal violet for 15 min at room temperature. The excess stain was washed three times with 200ll of PBS buffer. STEP 4: post-crystal violet, the wells were further subjected to air-dry for 15 min and the crystal violet in each well was solubilized by adding 200ll of 33% acetic acid. STEP 5: post-acetic acid[10].

2.4. Identification

The bacterial isolates exhibited having maximum waste water pollution reduction efficiency were recognized and isolated on the evidence of morphology, culture and their biochemical characteristics. The reference was taken from Bergey's Manual of Systematic Bacteriology and Probabilistic Identification of Bacteria (PIB) computer kit[11,12].

2.5. Morphological characteristics:

2.5.1. Gram staining- Gram staining was precisely performed with each and every step.

2.6. Cultural characteristics

2.6.1. Motility: Stabs of motility test agar medium were prepared and observed. Diffusion of the organism into the medium from the reference stab line indicated a positive test however; bacterial growth only along stab line without diffusion indicated a negative test[13].

2.7 Biochemical identification This test was done to determine the capability of an organism to utilize citrate as the sole source of carbon for metabolism with resulting alkalinity. A positive test was represented by the development of a deep blue color within 48 h indicating that organism has the ability to utilize the citrate while no change in color of the slants constituted a negative test[13].

2.7.1. Oxidase test: Cytochrome oxidase system is responsible for the Oxidase reaction. Blue color emergence within 1-2 min indicated a positive test and if no change occurs in the medium then it is a negative test[13].

Journal of Chemical Health Risks
www.jchr.org
JCHR (2025) 15(5), 2559-2570 | ISSN:2251-6727

2.7.2. Catalase test: Catalase test identifies and proves the presence of catalase enzyme. The bubbling (occurrence of oxygen) indicated a positive test while delayed or non-appearance of air bubbles confirmed the negative test[13].

2.7.3. Indole test: Bacteria oxidize tryptophan to form three metabolites namely, insole, skittle (methyl insole) and insole acetic acid (IAA). Appearance of red ring at the facet of the medium (alcoholic layer) showed a positive test while nonappearance of color suggested a negative test[13].

2.7.4. Methyl Red (MR) tests: A qualitative test for acid production (lactic, acetic and formic acid). Acid is produced from glucose via acid fermentation pathway. Production of a stable red color in the bacterial medium indicated adequate acid production and is considered a positive test, and a negative test gives yellow color to the medium[13].

2.7.5. Voges-Proskauer (VP) test: VP test is used to detect the formation of acetyl-methyl carbine from glucose fermentation. Formation of a bright pink color ring within 15 minutes of time indicated a positive result and dark brownish ring suggested a negative test[13].

2.7.8. Urease test: The ability of an organism to decompose urea can be determined by performing Urease Test. Color change in slants from yellow to dark pink or red indicated positive results while no change in color was recorded as negative result for unease test[13].

2.7.9 Triple sugar iron agar (TSI) test: The ability of an organism to uptake and incorporate a particular type of carbohydrate in a basal growth medium is determined by TSI test. It can be indicated with or without the production of gas. The production of hydrogen sulphide (H_2S) can also be determined along the side. The bacteria ferment the glucose producing CO2, and this can be identified by development of red color slant along with yellow color butt. The bacteria can ferment glucose and lactose and/or sucrose, and this can be confirmed by yellow color of slant and butt. If none of the glucose or sucrose is getting fermented, then it will form red color of slant and butt[13].

A) **Production of Gas:** If media gets cleaved or displaced at the bottom of the test tube, it confirms the presence of gas in the medium.

B) **Lead sulphide production:** Production of black colonies in the medium suggested a positive test for lead sulphide production.

C) H_2S production: If media turns black then it suggests a positive test while nonappearance of the black color indicated a negative test[13].

2.7.10. Malonate test: The capacity of an organism to utilize sodium malamute as their only source of carbon can be tested and confirmed with Malonate Test. This also results in alkalinity of the medium. The appearance of light blue to deep Prussian blue color all over the medium confirmed a positive test while nonappearance of the color suggested a negative test[13].

2.7.11. Carbohydrate utilization test: To discover the capacity of an organism to ferment a specific carbohydrate and integrate it in their basal medium can be confirmed using Carbohydrate utilization test. This test produces acid with or without visible gas. The presence of reddish orange to yellow color in the medium suggested a positive test while appearance of reddish pink color suggested a negative test[13].

2.7.12. Potassium cyanide test: This test is conducted to find out the capability of an organism to live and reproduce in presence of potassium cyanide. Their growth simply indicated a positive test[13].

2.7.13. Nitrate reduction test: To find out the ability of an organism to reduce nitrate to nitrite or free nitrogen, nitrate reduction test is performed. Development of pink or red color immediately suggested a positive test while no visible change in the medium's color indicated a negative test. A jot of nitrate-nitrite zinc free powder was incorporated to the tubes given negative results. No change in color of medium indicated absence of nitrate in the medium[13].

2.7.14. ONPG test: This test is performed to find out the presence or absence of the enzyme β-galactosidase in bacterial species. The bacteria can utilize o-nitrophenyl-β-D-galactopyranoside (ONPG). A color change in the broth of bacteria from color less to yellow suggested a positive test while no color change even after 24 h indicated a negative test[13].

2.8. Preparation of Leaf Broth Aqueous leaf derivative of *Costus igneus* was utilized to prepare AgNPs. The leaves were surface- sterilized, washed

Journal of Chemical Health Risks
www.jchr.org
JCHR (2025) 15(5), 2559-2570 | ISSN:2251-6727

with two times distilled water and air-dried at room temperature.20gm of finely chopped leaves were boiled in 200 ml deionized water for 30 minutes. The resulting extract to cool and filtered through the Whatman NO.1 filter paper and stored at 40ºC for further applications[14].

2.9. Green-synthesis of silver nanoparticles- 20 ml of *Costus* plant extract was added to 180 ml of 1 mM aqueous silver nitrate medium in500 ml flask under constant stirring. The reduction of Ag+ ions to Ag o was indicated by the color change from colorless to brown. The reaction mixture incubated at room temperature in a dark to minimize photo activation of silver nitrate. After complete reduction, the solution was centrifuged at 10,000rpm for 20 minutes. The supernatant was discarded, and the pellet was re-suspended in deionized water. This washing and centrifugation procedure was repeated two to three times remove any surface-absorbed impurities. The purified pellet was collected for subsequent characterization[15].

2.10. Characterization of synthesized AgNPs

2.10.1. UV-Visible Absorbance Spectroscopy: Suspension samples (0.5 mL) were analyzed at room temperature using a UV-Vis-spectrophotometer. The absorption spectra were recorded between 340 and 800 nm to follow the interaction of metal ions with the plant extract. The appearance of a surface plasmon resonance peak indicated the reduction of silver ions and nanoparticle formation within one hour. A control with only AgNO3, solution was also maintained.

2.10.2. Fourier Transforms Infrared Spectroscopy (FTIR): The nanoparticle solution was centrifuged at 10,000 rpm for 30 minutes, and the pellet was washed several times with deionized water to remove unbound biomolecules. The dried pellet was then analyzed using FTIR For spectrum collection, the freeze-dried powder was blended with potassium bromide (1:100) and compressed into a thin pellet. Spectra were recorded in the range of 4, 100400 cm using an FTIR spectrometer (Perkin Elmer).

2.10.3. X-Ray Diffraction: The crystalline structure of the nanoparticles was studied using an X-ray diffractometer equipped with Cuka radiation (A = 1.5406 A) at 40 kV and 30 mA, Data were collected over a 20 range of 20°-70° at a scan rate of 2" per minute. The average crystallite size was calculated from the broadening of diffraction peaks using the Debye-Scherrer equation:

$$D = K\lambda/\beta \cos\theta$$

where D is the crystallite size, K is the shape factor (0.94), A is the X-ray wavelength, f is the peak width at half maximum, and 9 is the Bragg angle.

2.10.4. Scanning Electron Microscopy- For SEM analysis, the pellet was processed by preparing thin films on a carbon-coated copper grid. A minute quantity of the sample was placed onto the grid, and any excess fluid was carefully absorbed with blotting paper. The grid was then air-dried before being subjected to SEM examination[16].

2.10.5. Antibacterial Assays- Antibacterial activity was assessed against common pathogenic bacteria include in *Bacillus subtilis, staphylococcus aureus, streptococcus pyogenes, Escherichia coli, Pseudomonas aeruginosa, and Klebsiella aerogenes* using the disc diffusion technique. Bacterial cultures were grown in Luria Bertani (LB) broth/agar medium, and fresh overnight cultures were spread uniformly on Mueller Hinton Agar (MHA) plates. Sterile filter paper discs (5 mm diameter) impregnated with silver nanoparticles (30 g/mL) were placed on the plates along with antibiotic-loaded discs (30 g/mL) as positive control. The plates were inhibition surrounding the discs were measured.

2.10.6. Biofilm Inhibition Assay- The inhibitory effect of silver nanoparticles (AgNPs) on bacterial and fungal biofilm development was determined by adapting the colony biofilm method[17]. Briefly, UV-sterilized membranes were placed on agar medium and inoculated with 10 mL of diluted planktonic culture together with 100 mL of AgNPs suspensions at varying concentrations (100, 250, 500, and 1000 mg/mL). For controls, biofilm-coated membranes were transferred to fresh agar plates and treated with 100 mL sterile phosphate-buffered saline (PBS). All plates were incubated for 24 hours under the same experimental conditions as the colony biofilm model. Each experiment was performed in triplicate to ensure reproducibility.

Journal of Chemical Health Risks
www.jchr.org
JCHR (2025) 15(5), 2559-2570 | ISSN:2251-6727

3. Results

3.1 Characterization of Gram-Negative Bacteria from UTI Patient samples In recent study gram negative bacteria isolated from UTI Patient samples OF JNUIMSRC and are grown on agar medium for the further analysis.

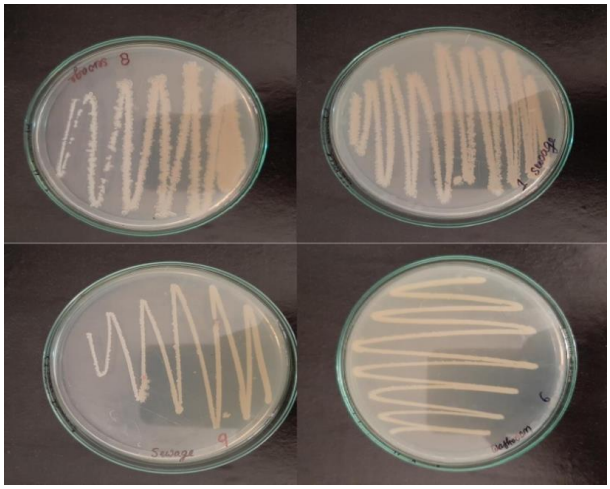

Fig 3.1.1Pure cultures of indigenous bacterial isolates

In the present study 3 isolates of Gram positive and 8 Gram negative bacteria were detected respectively.

Table 1: Details of morphological characteristics of isolated bacteria

Date of isolation		CFU/ ml	Colony on NAM	texture	configuration	margin	Elevation	Gram reaction	Shape of isolate
10/02/2024	SewageS1	7.8 X 10^2	Off white	smooth	Circular	Irregular	Raised	negative	rod
	S2	4.8 X 10^3	Pink	rough	Circular	Irregular	Raised	negative	rod
	S3	3.4 X 10^6	Pale	rough	Circular	Regular	Raised	positive	cocci
12/02/2024	Sewage4	6.8 X 10^3	Off white	smooth	Circular	Irregular	Raised	negative	rod
	S5	7.2 X 10^7	Mucoid	Rough	Circular	Irregular	convex	positive	cocci
	S6	5.9 X 10^2	Mucoid	smooth	Lobate	Irregular	Raised	negative	rod
14/02/2024	Washroom	0.2 X 10^2	Light orange	rough	Lobate	Irregular	Raised	negative	rod
	W2	1.8 X 10^2	white	smooth	Circular	Irregular	Raised	Positive	cocci
	W3	3.5 X10^2	Cream	rough	Circular	Irregular	Raised	negative	rod
	W4	3.8 X 10^3	Orangish	rough	Circular	Irregular	Raised	negative	rod

3.2 Biofilm formation

Silver nanoparticles have also been tested for their anti-biofilm activity against biofilm producing bacteria. In this study, the in vitro biofilm-inhibitors effect of AgNPs was assessed in a concentration-dependent manner against the biofilm- forming bacteria 1, 3A, 3B, 7, and9.

Table 2: - Biofilm formation by different isolates at different concentration of AgNPs and Anibiotics (Colistin)

Isolate no.	Concentration	OD (in nm)	Biofilm Formation
1	10 µl	- 1.781	Strong
	20 µl	1.862	Moderate
	30 µl	2.812	Moderate
	40 µl	1.90	Moderate
	50µl	-	Moderate
	Antibiotic		Strong
3A	10 µl	2.266	Moderate
	20 µl	2.60	Moderate
	30 µl	0.86	Weak
	40 µl	1.967	Moderate
	50µl	-	Strong
	Antibiotic	-	Strong
3B	10 µl	1.859	Moderate
	20 µl	1.220	Weak
	30 µl	1.95	Moderate
	40 µl	1.990	Moderate
	50µl	0.648	Moderate
	Antibiotic	-	Strong
7	10 µl	0.977	Weak
	20 µl	1.816	Moderate
	30 µl	1.596	Weak
	40 µl	1.448	Weak
	50µl	2.75	Moderate
	Antibiotic	2.672	Moderate
9	10 µl	1.594	Weak
	20 µl	1.798	Moderate
	30 µl	2.317	Moderate
	40 µl	-	Strong
	50µl	-	Strong
	Antibiotic	-	Strong

The bacteria were cultured and treated with 10–50 µg/ml of the separately synthesized AgNPs combination with the Antibiotic. The outcomes of the assay demonstrated that the biologically produced AgNPs inhibited biofilm formation by the bacterial strains. The MICs of the anti-biofilm effect were represented in terms of IC50 and all AgNPs, regardless of the employed in their fabrication, displayed an excellent MIC value against biofilm formation.

ODc = Average OD of negative control + (3x standard

Journal of Chemical Health Risks
www.jchr.org
JCHR (2025) 15(5), 2559-2570 | ISSN:2251-6727

deviation (SD) of negative control)

OD isolate = Average OD of isolate – ODc

Table3: -Biofilm formation by different isolates

Biofilm formation	Percentage of isolates	No. of isolates
Nonadherent	0%	0
Weak	20%	6
Moderate	53 %	16
Strong	26.6 %	8

Total=30 isolates of different concentrations

3.3 Plant (*Costus igneus)*

Various pharmacological studies have shown that the plant extract of *Costus igneus*is non-toxic and have anti-diabetic, anti-inflammatory, angiokinetic and antipyretic effect, antiulcerogenic potential, antidiarrheal activity, diuretic activity, contraceptive efficiency, antarthritic activity[18].

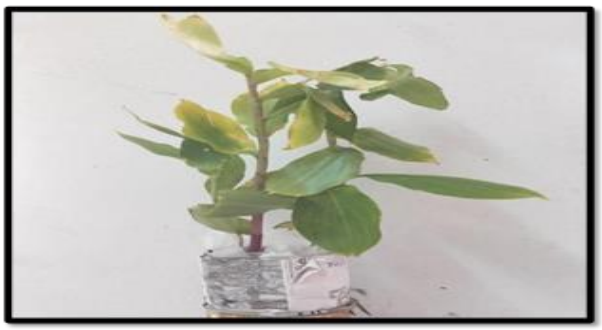

Fig 3.3.1 *Costus igneus* (Insulin plant): Plant used to synthesize silver nanoparticle

3.4 Synthesis of silver nanoparticles: - With the addition of plant derivatives of *Costus igneus* to AgNO 3 solution, color was changed from whitish to brown (Fig.). This transformation in color resulted from the reduction of silver ions, confirming the formation of AgNPs. After 3 days of incubation the fully reduced nanoparticles were observed and centrifugation at 10,000 rpm for 20 minutes. The supernatant was collected and preserved at freezing temperature for subsequent applications[19].

Fig 3.4.1. Color change observation at different concentration (1:9,2:8) along with control (Left to right)

3.5. UV-VIS Spectroscopy

The progression of the reaction between metal ions and the leaf derivative was observed by UV-Visible spectroscopy of silver nanoparticles in aqueous medium, across different wavelengths ranging from 340 to 800 nm. The reduction of silver ions and generation of silver nanoparticles occurred took place one hour of the reaction. A Control was maintained using AgNO3[20]. The green-fabricated AgNPs initially showed a yellowish color in aqueous medium owing to excitation of surface plasmon resonance of AgNPs. Then solution's color shifted from yellowish to brown on addition of plant derivative to silver nitrate. This alteration in color signified the successful formation of AgNPs[21]. verification of AgNPs formation was established through an absorbance observed between 430 to 460nm. Color change in the reaction mixture occurred over time. The metabolites present in the leaf derivative function as electron donor and reducing Ag+ ions in elemental silver. Silver nanoparticles were produced using the plant extract of *Costus igneus,* where in silver nitrate was reduced to form AgNPs[22]..

The synthesized silver nanoparticles were characterized by UV-Spectrometer within the wavelength range of 300-700nm. The synthesized AgNPs (silver nanoparticles) from plant extract of *Costusn igneus* were characterized using UV-visible spectroscopy, Fourier Transform Infrared spectroscopy, Scanning electron microscopy (SEM), and X-ray diffraction analysis. As well as antibacterial and anti-biofilm activities were analyzed and evaluated. The characterization of [AgNPs]. UV-vis using UV Visible absorption spectrophotometer. The OD was taken

Journal of Chemical Health Risks
www.jchr.org
JCHR (2025) 15(5), 2559-2570 | ISSN:2251-6727

between 300-800 nm but the peak was obtained between400-480 nm. The graphs were plotted as per the values obtained[23].

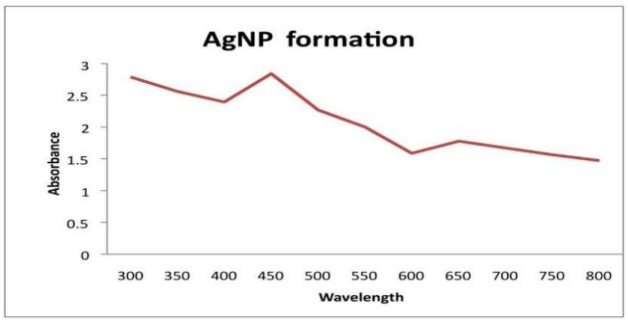

Fig.3.5. UV-Vis spectrum of synthesized AgNPs at different wavelengths

3.6 Fourier transform infrared (FTIR)

For FT-IR analysis, a 0.5g sample of AgNPs was used, and the spectra was recorded in the range of 4000–400 cm -1 at a resolution of 4 cm -1 to identify the chemical functional groups present on the surface of green- synthesized AgNPs[24]. The FT-IR spectrum shows the presence of bands at 3356, 2886, 2818, 2102, 1637,1406, and 580cm -1 corresponding to monosubstituted amide, nitro, primary amide, carboxylic, as well as alcohol functional group, respectively. For FT-IR analysis, the synthesized silver nanoparticles solution was centrifuged at10,000 rpm for 30 minutes. The resulting pellet was washed three times with 5 mL of deionized water to remove any unbound proteins or enzymes that are not capping the silver nanoparticles. The pellet was then dried using a vacuum dryer. It was analyzed by FTIR[25].

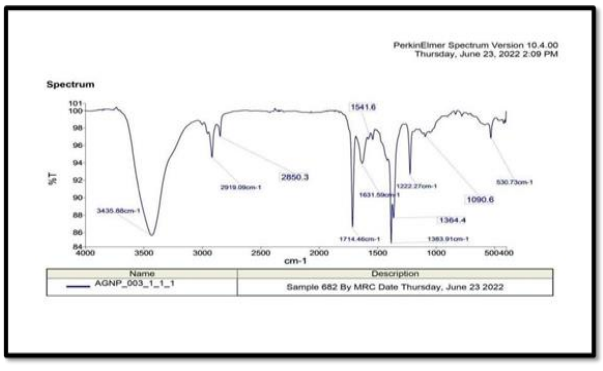

Fig.3.6 FT-IR spectrum of biosynthesized AgNPs

3.7 Field Emission Scanning Electron Microscopy (FESEM)

The pellet was prepared for FESEM analysis. The Integration of SEM with energy-dispersive X-ray spectroscopy (EDX) allows the examination morphology silver nanoparticles as well as the determination of their element composition.

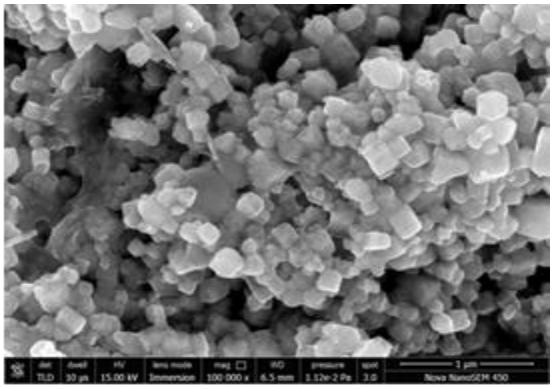

Fig.3.7.1.SEM micrograph of silver nanoparticles synthesizes from *Costus igneus*

SEM was used to study particle morphology, and size distribution was obtained using manual measurements or specialized. Combined with energy-disperse X-ray spectroscopy (EDX), it also provides elemental composition analysis of the silver nanoparticles. The combination of SEM with energy-dispersive X-ray spectroscopy (EDX) can be used to examine silver powder morphology and also conduct chemical composition analysis. The limitation of SEM is that it is not able to resolve the internal structure, but it can provide valuable information regarding the purity and the degree of particle aggregation. The modern high-resolution SEM is able to identify the morphology of nanoparticles below the level of 10 nm[26].

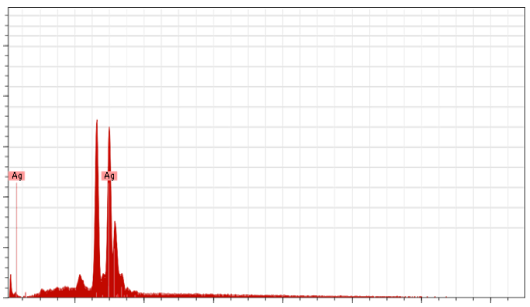

Fig.3.7.2 SEM Analysis: graph showing confirmation of Ag

Journal of Chemical Health Risks
www.jchr.org
JCHR (2025) 15(5), 2559-2570 | ISSN:2251-6727

3.8 X-Ray diffraction analysis (XRD)

The principle of X-ray diffraction [XRD] is based on Bragg's law. XRD, typically is based on the wide-angle elastic scattering of X-rays. It can be used to determine the degree of crystallinity [27]. isomorphous substitutions, particle sizes[28]. and other structure When X-rays are reflects on a crystal, they produce multiple diffraction patterns, that reflect the physio-chemical properties of the crystal structures. In a powdered sample, the diffracted beams arise material itself, revealing its structural characteristics. consequently, XRD is widely employed to analyze the structural features of divers' materials, including inorganic catalysts, superconductors, bio-molecules, glasses, polymers. The analysis depends on interpretation the diffraction patterns. As each material generate a unique diffraction profile that can be define and identify by composition with reference data in the Joint Committee on Powder Diffraction Standards (JCPDS) database[29].

This method has been used to measure phase identification, conduct quantitative analysis, and to determine structure imperfections in samples from various disciplines, such as geological, polymer, environmental, pharmaceutical, and forensic sciences. Recently, the applications have extended to the characterization of various nano- materials and their properties.The working principle of X-ray diffraction is Bragg's law. Typically, XRD is based on the wide-angle elastic scattering of X-rays. Although XRD has several merits, it has limited disadvantages, including difficulty in growing the crystals and the ability to get results pertaining only to single conformation/binding state Another drawback of XRD is the low intensity of diffracted X- rays compared to electron diffractions[30].

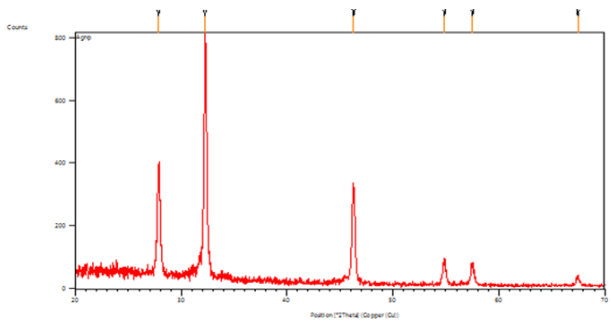

Fig.3.8 X-ray diffraction pattern of synthesized AgNPs

3.9 Antibacterial activity

AgNPs appear to be potential antibacterial agents owing to their high surface-to-volume ratios and crystalline surface structure. *E.coli* cells exposed to AgNPs exhibited accumulation of nanoparticles in the cell wall, resulting in the formation of "pits" that ultimately caused cell death. The various isolates were cultured on Muller- Hinton Agar [MHA] medium using disc method. The disc measuring5mm in size were dipped in AgNPs (5µl) and placed on the plate. Similarly, plant extract and antibiotic discs were also placed along with the control (without any of them) which was dipped in double distilled water[31]. The inhibition zones were measured and tabulated, AgNPs showed the potentially better results than antibiotics and plant extract. The zones were formed as in Fig.

Biologically synthesized AgNPs from the culture supernatants of *Klebsiella pneumoniae* were evaluated; the efficiencies of various antibiotics, such as penicillin G, amoxicillin, erythromycin, clindamycin, and vancomycin against *Staphylococcus aureus* and *E. coli* were increased in the presence of Ag-NPs. When compared to AgNPs, hydrogel–silver nanocomposites showed excellent antibacterial activity against *E. coli*. One-pot synthesis of chitosan–Ag–nanoparticle composite was found to have higher antimicrobial activity than its components at their respective concentrations, because one-pot synthesis favors the formation of small AgNPs attached to the polymer, which can be dispersed in media of pH $\leq$ 6.3[32]. Biologically produced AgNPs using culture supernatants of *Staphylococcus aureus* showed significant antimicrobial activity against methicillin-resistant *S. aureus*, followed by methicillin- resistant *Staphylococcus epidermidis* and *Streptococcus pyogenes*, whereas only moderate antimicrobial activity was observed against *Salmonella typhi* and *Klebsiella pneumoniae*. The mechanisms of AgNP-induced cell death was observed in *E. coli* through the leakage of reducing sugars and proteins. Furthermore, AgNPs are able to destroy the permeability of the bacterial membranes via the generation of many pits and gaps, indicating that AgNPs could damage the structure of the bacterial cell membrane. Silver nanocrystalline chlorhexidine (AgCHX) complex showed strong antibacterial activity against the tested Gram-positive/negative and methicillin- resistant *Staphylococcus aureus* (MRSA) strains. Interestingly, the minimal inhibitory concentrations (MICs) of

Journal of Chemical Health Risks
www.jchr.org
JCHR (2025) 15(5), 2559-2570 | ISSN:2251-6727

nanocrystalline Ag(III)CHX were much lower than those of the ligand (CHX), $AgNO_3$, and the gold standard, silver sulfadiazine. Biofilms are not only leads to antimicrobial resistance, but are involved in the development of ocular-related infectious diseases, such as microbial keratitis. Similarly, guava leaf extract reduced AgNPs (Gr-Ag-NPs) showed significant antibacterial activity and stability against *E. coli* compared to chemically synthesized AgNPs; the reason for this higher activity could be the adsorption of biomolecules on the surface of the Gr-Ag-NPs.

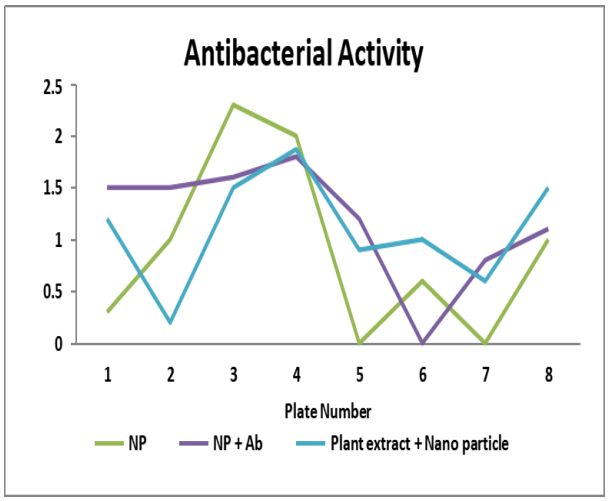

Fig.3.9.1. Antibacterial activity of AgNPs synthesize from plant extract of *Costus igneus*

3.10 Biofilm inhibition- Two of the selected set of antibiotics and nanoparticle and nanoparticle alone have shown the maximum inhibition activity against the biofilm of uropathogens. The methanolic extract of insulin plant efficiently inhibits biofilm formation where 81% inhibition. Additionally, the least activity was observed in extracted plant sample. Additionally, the least activity was observed in extracted plant sample. Previous studies revealed a strong evidence that the medicinal plants have promising attitude to combat various types of infectious diseases caused by numerous microbial species. Medicinal plants attribute well to cure various diseases due to their antibacterial potential such as B. ciliate, *Jasminum officinale, Santalum album, Oxalis corniculata, Artemisia vulgaris, Cinnamomum tamala*, and *Ageratina adenophora*. Similarly, various ethanolic extracts belong to family Meliaceae, Piperaceae and Sapindaceae interfered with the bacterial QS molecules that inhibit the formation of biofilm. Quorum sensing molecules such as acyl homoserine lactones (AHLs) in *P. aeruginosa*, play important role in release of virulence and toxin is one of the strategy to control its pathogenicity. Medicinal plants have numerous phytochemicals like phenolics, flavonoids, quinones, alkaloids, terpenoids, and polystyrenes that play a key role against microbial pathogenicity and proved to be involved in inhibition of QS molecules as well as biofilm[33].

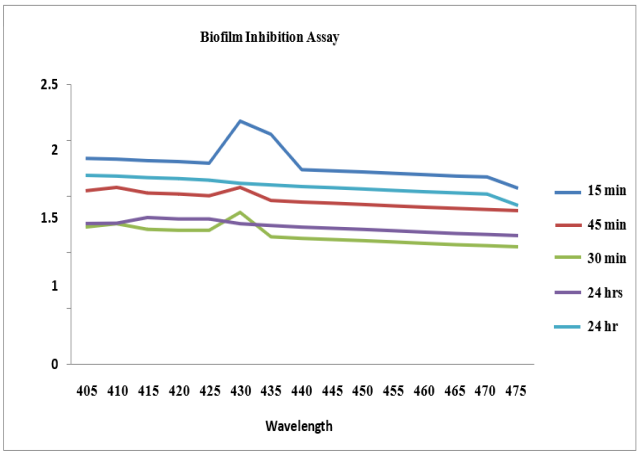

Fig.3.10Anti-biofilm activity of AgNPs against UTI causing bacteria

Biofilm-formed enterococcal urinary tract isolates (n = 12) were used for studying the antibiofilm activity of plant extract of *Costus igneus*, Ciproflaxin and chemical AgNPs. The average particle sizes of *Costus igneus* AgNPs were in between 65-150nm, respectively. The results of Fourier transform infrared analysis revealed that phytocompounds, were the main compounds incorporated in the synthesis of AgNPs using plant extract respectively. The purity and crystalline nature of the AgNPs have been confirmed by X-ray Diffraction analysis. The results of antimicrobial activity showed that MIC of synthesized AgNPs were 37.64, 725.7, and 61.08 µg/ml, respectively. sub-MIC values the results revealed that it was concentration dependent. Therefore, further studies were carried out to evaluate the antibiofilm activity of AgNPs at a concentration of 10,20,30,40 & 50 µg/ml. The results showed that AgNPs reduced the formed biofilm to 81% as compared to that of the control, while plant extract showed no significant activity. Accordingly, *Costus igneus* AgNPs had the most potent antibacterial activity against biofilm-associated enterococcal isolates. Although NPs have the potential to treat and diagnose UTIs, there are still

Journal of Chemical Health Risks

www.jchr.org

JCHR (2025) 15(5), 2559-2570 | ISSN:2251-6727

several challenges that need to be addressed prior to their successful translation in the clinics including the investigation of the interaction between NPs and cells, tissues, and organs, the identification of the most appropriate routes of administration, and most importantly the evaluation of toxic responses to long-term exposure to NPs. [34]. Despite several advancements regarding the value of NPs in the diagnosis and treatment of UTIs, it will be important to examine the pathways through which NPs exert their therapeutic efficacy. There is also limited information on the metabolism and clearance of NPs and on the nature of their targets[35]. The specific combination of NPs and antimicrobials may reduce the emergence of multidrug resistance of bacteria to drug sensitivity and translation to clinical practice will require a thorough investigation of the pharmacokinetic and pharmacodynamic profiles of these NPs. Finally, for innovative research, the limits of pathogen detection and the time of the proposed analysis will have to be significantly improved.

4. Conclusion and Future Aspect

Recent study shows that *Costus igenus* has many benefits as its own and when the plant extract is made into nanoparticles along with silver, its benefits increase. Due to high surface to volume ration AgNPs acts as a strong antibiofilm agent shown to reduce the biofilm formation to 80% when studied with the pathogens having potential to cause UTIs. Although nanoparticles have the potential to treat and diagnose UTIs, there are still several challenges must be addressed before clinical translation. These include understanding NP interaction with cells, tissues, and organs, determining optimal administration routes, and critically, evaluating to long-term toxic. Despite advancements in NP-based UTI therapies, the mechanisms underlying their therapeutic effect remain unclear. limited information is available on the NP metabolism and clearance and specific targets. Combining NPs with antimicrobial may help reduce multi-drug resistance, but clinical translation will require thorough pharmacokinetic and pharmacodynamic studies. Additionally, improvements in pathogen detection sensitivity and analysis speed are essential for innovative diagnostic approaches.

4. ACKNOWLEDGMENT

Concept and design: - Shivani Kumari (SK) Dr. Kratika Pathak (KP) Divya Shrivastava [DS]

Draft: - Swati Verma [SV], Uzma Patel [UP]

Experimentation: - Ruchika Bhadani [RB], Abhishek Kumar [AK]

5. CONFLICT OF INTEREST

No conflict of interest.

6. FUNDING SOURCE

Financial Help was provided by EDIIC JNU Jaipur and Reference bacterial cultural was procured from BIOBANK Jaipur national University Jaipur

Refrences

1. Zhou Y, Zhou Z, Zheng L, Gong Z, Li Y, Jin Y, Huang Y, Chi M. Urinary Tract Infections Caused by Uropathogenic *Escherichia coli*: Mechanisms of Infection and Treatment Options. Int J Mol Sci. 2023 Jun 23;24(13):10537. doi: 10.3390/ijms241310537. PMID: 37445714; PMCID: PMC10341809.
2. He Y, Zhao J, Wang L, Han C, Yan R, Zhu P, Qian T, Yu S, Zhu X, He W. Epidemiological trends and predictions of urinary tract infections in the global burden of disease study 2021. Sci Rep. 2025 Feb 8;15(1):4702. doi: 10.1038/s41598-025-89240-5. PMID: 39922870; PMCID: PMC11807111
3. Li X, Fan H, Zi H, Hu H, Li B, Huang J, Luo P, Zeng X. Global and Regional Burden of Bacterial Antimicrobial Resistance in Urinary Tract Infections in 2019. J Clin Med. 2022 May 17;11(10):2817. doi: 10.3390/jcm11102817. PMID: 35628941; PMCID: PMC9147874.
4. Conway C, Beckett MC, Dorman CJ. The DNA relaxation-dependent OFF-to-ON biasing of the type 1 fimbrial genetic switch requires the Fis nucleoid-associated protein. Microbiology (Reading). 2023 Jan;169(1):001283. doi: 10.1099/mic.0.001283. PMID: 36748578; PMCID: PMC9993118.
5. Jin X, Marshall JS. Mechanics of biofilms formed of bacteria with fimbriae appendages. PLoS One. 2020 Dec 8;15(12):e0243280. doi: 10.1371/journal.pone.0243280. PMID: 33290393; PMCID: PMC7723297.

Journal of Chemical Health Risks

www.jchr.org

JCHR (2025) 15(5), 2559-2570 | ISSN:2251-6727

6. Jiang X, Hall AB, Arthur TD, Plichta DR, Covington CT, Poyet M, Crothers J, Moses PL, Tolonen AC, Vlamakis H, Alm EJ, Xavier RJ. Invertible promoters mediate bacterial phase variation, antibiotic resistance, and host adaptation in the gut. Science. 2019 Jan 11;363(6423):181-187. doi: 10.1126/science.aau5238. PMID: 30630933; PMCID: PMC6543533
7. Zamora M, Ziegler CA, Freddolino L, Wolfe AJ. A Thermosensitive, Phase-Variable Epigenetic Switch: pap Revisited. Microbiol Mol Biol Rev. 2020 Jul 29;84(3):10.1128/mmbr.00030-17. doi: 10.1128/MMBR.00030-17. PMID: 32727743; PMCID: PMC7392537.
8. Hegde PK, Rao HA, Rao PN. A review on Insulin plant (*Costus igneus Nak*). Pharmacogn Rev. 2014 Jan;8(15):67-72. doi: 10.4103/0973-7847.125536. PMID: 24600198; PMCID: PMC3931203
9. Dinh A, Duran C, Hamami K, Afif M, Bonnet F, Donay JL, Lafaurie M, Chartier-Kastler E (2022) Hyaluronic Acid and Chondroitin Sulphate Treatment for Recurrent Severe Urinary Tract Infections due to MultidrugResistant Gram-Negative Bacilli in a Patient With Multiple Sclerosis: Case Report and Literature Review. Open forum infectious diseases 9 (7): ofac245
10. Gomes LC, Moreira JM, Simões M, Melo LF, Mergulhão FJ. Biofilm localization in the vertical wall of shaking 96-well plates. Scientifica (Cairo). 2014;2014:231083. doi: 10.1155/2014/231083. Epub 2014 Apr 13. PMID: 24834360; PMCID: PMC4009116.
11. Krieg, N. R.; Holt, J. G., Eds. Bergey's Manual of Systematic Bacteriology, 1st ed.; Williams & Wil kins: Baltimore, 1984; Vol. 1.
12. Janda, J. M.; Abbott, S. L. The Enterobacteria, 2n d ed.; ASM Press: Washington, DC, 2006.
13. Mac Faddin, J. F. Biochemical Tests for Identifica tion of Medical Bacteria, 2nd ed.; Williams & Wil kins: Baltimore, MD, 1980.
14. Ali, M. A.; Ahmed, T.; Khan, S. T.; Abdin, M. Z. Green synthesis of copper nanoparticles using Euc alyptus leaf broth: Evaluation of their innate anti microbial and catalytic activities. J. Photochem. P hotobiol., B 2015, 146, 1–9.
15. Nalawade, P.; Mukherjee, P.; Kapoor, S. Biosynth esis, characterization and antibacterial studies of s ilver nanoparticles using pods extract of Acacia a uriculiformis. Spectrochim. Acta, Part A 2014, 12 9, 121–124.
16. Savithramma, N.; Linga Rao, M.; Suvarnalathadevi, P. Evaluation of antibacterial efficacy of biologically synthesized silver nanoparticles using stem barks of *Boswellia ovalifoliolata* Bal. and Henry and *Shorea tumbuggaia* Roxb. *J. Biol. Sci.* 2011, *11*, 39–45.
17. Anderl, J. N.; Franklin, M. J.; Stewart, P. S. Role of Adhesion in the Virulence of *Pseudomonas aeruginosa* Biofilms. *J. Infect. Dis.* 2000, *182*, 1660–1668.
18. Srivastava S, Singh P, Jha KK, Mishra G, Srivastava S, Khosa RL. Antiinflammatory, Analgesic and Antipyretic Activities of Aerial Parts of Costus speciosus Koen. Indian J Pharm Sci. 2013 Jan;75(1):83-8. doi: 10.4103/0250-474X.113532. PMID: 23901165; PMCID: PMC3719154
19. Farzeen, Sana & Kumar, Ajay. (2022). Synthesis of silver nanoparticles (AgNPs) of leaves extract of Rhynchoglossum notonianum wall. for enhancing its bioavailability and antibacterial activity. International journal of health sciences. 6947-6961. 10.53730/ijhs.v6nS2.6756.
20. Sudeep, P. K.; Ipe, B. I.; Thomas, K. G. DNA-Mediated Dimerization of Gold Nanorods: A Spectroscopic Tool for DNA Sensing. *J. Phys. Chem. B* 2005, *109* (25), 12130–12135.
21. Abbas, Q.; Saleem, M.; Phull, A. R.; Rafiq, M.; Hassan, M.; Lee, K.-H.; Seo, S.-Y. Green Synthesis of Silver Nanoparticles using Bidens Frondosa Extract and their Tyrosinase Activity. Iran. J. Pharm. Res. 2017, 16 (2), 763–770
22. Ashraf JM, Ansari MA, Khan HM, Alzohairy MA, Choi I. Green synthesis of silver nanoparticles and characterization of their inhibitory effects on AGEs formation using biophysical techniques. Sci Rep. 2016 Feb 2;6:20414. doi: 10.1038/srep20414. PMID: 26829907; PMCID: PMC4735866.
23. Ansari M, Ahmed S, Abbasi A, Khan MT, Subhan M, Bukhari NA, Hatamleh AA, Abdelsalam NR. Plant mediated fabrication of silver nanoparticles, process optimization, and impact on tomato plant. Sci Rep. 2023 Oct 23;13(1):18048. doi: 10.1038/s41598-023-45038-x. PMID: 37872286; PMCID: PMC10593853.
24. Suregal, R.; Yadav, A.; Pande, S. Synthesis of Chitosan-Stabilized Silver Nanoparticles for Enhanced Antibacterial Activity. *J. Agric. Food Chem.* 2020, *68* (15), 4330–4338.

25. Hasan SM, Hussain S, Yousuf M, Tapia-Hernández JA, Raja DA. Protein-Based Silver Nanoparticles: Synthesis, Characterization, Administration, and Nanomedicine Applications. Int J Biomater. 2025 May 26;2025:5533798. doi: 10.1155/ijbm/5533798. PMID: 40458607; PMCID: PMC12129617.
26. Abouzeid, R. E., M. E. Owda, and S. Dacrory. 2022. "Effective Adsorption of Cationic Methylene Blue Dye on Cellulose Nanofiber/Graphene Oxide/Silica Nanocomposite: Kinetics and Equilibrium." Journal of Applied Polymer Science 139, no. 25
27. Dey, A.; Sen, B.; Ghosh, P.; et al. Green Synthesis of Silver Nanoparticles Using Plant Extract and Their Antimicrobial Efficacy. *ACS Nano* 2009, *3* (10), 3121–3129.
28. Hiremath, S.; Vidya, C.; Lourdu Antonyraj, M. A.; Chandraprabha, M. N.; Gandhi, P.; Jain, A.; Anand, K. Biosynthesis of ZnO Nanoparticles Assisted by Euphorbia tirucalli (Pencil Cactus). Int. J. Curr. Eng. Technol. **2013**, 1 (4), 176–179
29. Omori NE, Bobitan AD, Vamvakeros A, Beale AM, Jacques SDM. Recent developments in X-ray diffraction/scattering computed tomography for materials science. Philos Trans A Math Phys Eng Sci. 2023 Oct 30;381(2259):20220350. doi: 10.1098/rsta.2022.0350. Epub 2023 Sep 11. PMID: 37691470; PMCID: PMC10493554.
30. Ali, A., Chiang, Y. W., & Santos, R. M. (2022). X-ray Diffraction Techniques for Mineral Characterization: A Review for Engineers of the Fundamentals, Applications, and Research Directions. Minerals, 12(2), 205. https://doi.org/10.3390/min12020205
31. Tahan M, Zeraatkar S, Neshani A, Marouzi P, Behmadi M, Alavi SJ, Hashemi Shahri SH, Hosseini Bafghi M. Antibacterial Potential of Biosynthesized Silver Nanoparticles Using Berberine Extract Against Multidrug-resistant Acinetobacter baumannii and Pseudomonas aeruginosa. Indian J Microbiol. 2024 Mar;64(1):125-132. doi: 10.1007/s12088-023-01136-y. Epub 2023 Nov 27. PMID: 38468728; PMCID: PMC10924866
32. Zhang XF, Liu ZG, Shen W, Gurunathan S. Silver Nanoparticles: Synthesis, Characterization, Properties, Applications, and Therapeutic Approaches. Int J Mol Sci. 2016 Sep 13;17(9):1534. doi: 10.3390/ijms17091534. PMID: 27649147; PMCID: PMC5037809
33. Miranda SW, Asfahl KL, Dandekar AA, Greenberg EP. Pseudomonas aeruginosa Quorum Sensing. Adv Exp Med Biol. 2022;1386:95-115. doi: 10.1007/978-3-031-08491-1_4. PMID: 36258070; PMCID: PMC9942581
34. Qindeel M, Barani M, Rahdar A, Arshad R, Cucchiarini M. Nanomaterials for the Diagnosis and Treatment of Urinary Tract Infections. Nanomaterials (Basel). 2021 Feb 22;11(2):546. doi: 10.3390/nano11020546. PMID: 33671511; PMCID: PMC7926703.
35. Kim YJ, Tae BS, Bae JH. Cognitive Function and Urologic Medications for Lower Urinary Tract Symptoms. Int Neurourol J. 2020 Sep;24(3):231-240. doi: 10.5213/inj.2040082.041. Epub 2020 Sep 30. PMID: 33017894; PMCID: PMC7538292